Mixing process of two miscible fluids in a lid-driven cavity

Fenglei Huang, Dengfei Wang, Zhipeng Li, Zhengming Gao, J.J. Derksen

PII: S1385-8947(19)30030-0
DOI: https://doi.org/10.1016/j.cej.2019.01.024
Reference: CEJ 20745

To appear in: *Chemical Engineering Journal*

Received Date: 20 July 2018
Revised Date: 1 December 2018
Accepted Date: 4 January 2019

Please cite this article as: F. Huang, D. Wang, Z. Li, Z. Gao, J.J. Derksen, Mixing process of two miscible fluids in a lid-driven cavity, *Chemical Engineering Journal* (2019), doi: https://doi.org/10.1016/j.cej.2019.01.024

Mixing process of two miscible fluids in a lid-driven cavity

Fenglei Huang [a,b], Dengfei Wang[d], Zhipeng Li [a,b,*], Zhengming Gao [a,b,*], J.J. Derksen [c]

[a] Beijing Advanced Innovation Center for Soft Matter Science and Engineering, Beijing University of Chemical Technology, Beijing 100029, China

[b] State Key Laboratory of Chemical Resource Engineering, School of Chemical Engineering, Beijing University of Chemical Technology, Beijing 100029, China

[c] School of Engineering, University of Aberdeen, Aberdeen AB24 3UE, UK

[d] Daqing Petrochemical Research Center, Petrochemical Research Institute, China National Petroleum Corporation, Daqing City, Heilongjiang Province 163714, China

* Corresponding author. Tel.: +8610 64418267; fax: +8610 64449862. E-mail address: lizp@mail.buct.edu.cn (Zhipeng Li), gaozm@mail.buct.edu.cn (Zhengming Gao).

Abstract

A laminar lid-driven cavity flow was constructed to represent the fundamental characteristics of an industrial dynamic mixer. The flow patterns and mixing process in the cavity were measured by using particle image velocimetry (PIV) and planar laser-induced fluorescence (PLIF) experiments respectively. The refractive indices of the two miscible liquids involved were carefully matched to allow for unhindered optical access. The mixing process was predicted by using computational fluid dynamics (CFD) including models for species transport. The simulated flow and mixing results are in good agreement with the experimental data. The effects of density difference and viscosity of the two miscible fluids on the mixing process were evaluated. Minor variations in the densities of the fluids have significant influence on the mixing process in terms of the coefficient of variation as a function of time. The dimensionless group $\frac{Ar}{Re}$ (Archimedes number over Reynolds number) is proposed to characterize the mixing process in the cavity.

Keywords: mixing of miscible fluids; particle image velocimetry; planar laser-induced fluorescence; lid-driven cavity flow; Species transport model

Highlights:

- Refractive index matching method was used to enable flow and mixing visualization
- The dynamic mixing process from layering to blending was quantitatively measured
- Simulated velocity and concentration fields agree well with the experimental data
- The dimensionless group of $\frac{Ar}{Re}$ is proposed to characterize the mixing process in the cavity

Introduction

Dynamic mixers for blending polymers are commonly used in chemical, plastic and rubber industries [1-2]. Over the last decades, only few works about dynamic mixers can be found in the literature. The dynamic mixer was invented in the 1980s by Gale at Rapra Technology Limited [1], and it is often used as an add-on unit to existing extruders to improve dispersive mixing. Due to complex geometry (for example, Fig. 1) and transient flow characteristics, it is not an easy task to obtain the flow and mixing characteristics in a dynamic mixer by visualization technologies. Most of the studies on dynamic mixers were performed by using computational fluid dynamics (CFD) methods. Wang and Manas-Zloczower first characterized the three-dimensional flow field of a dynamic mixer by using a fluid dynamics analysis package based on the finite element method and discussed the potential use for dispersive mixing [3]. A more specific and quantitative mixing analysis was proposed by Woering et al. who used a two-dimensional approximation for the device [4]. Recently, comprehensive three-dimensional simulations have been performed by Grosso et al. [5]. In their work, a non-dimensional number *k* (the ratio between the axial and the tangential velocity of the fluid at the inlet) and the number of cavities per row were found to be the key factors for performance of the dynamic mixer.

In producing fibers with different colors or functions in industries, it is necessary to uniformly disperse colorful or functional master batches (i.e., a small amount of polymer containing functional particles) into raw polymer. The master batches usually have different densities from the raw polymer. Different temperatures are often required to add different kinds of master batches into the raw polymer. The effects of density difference and viscosity on mixing therefore deserves more attention. So far, all the existing work on dynamic mixers did not involve these influencing factors; effects of density difference and viscosity on mixing performance are considered for the first time in this study.

The dynamic mixer (Fig. 1) was simplified to a lid-driven cavity flow model (Fig. 2) in this work, because the liquid in the cavities of the dynamic mixer is sheared due to the relative motion of the rotor and the stator, which is similar to the process where a moving lid shears the liquid in a lid-driven cavity. Lid-driven cavity flow has long been considered as an ideal model for benchmarking Navier–Stokes numerical solvers, and this flow configuration is the simplest one for analyzing the flow which occurs in important industrial processes, e.g. chemical etching [6], film coating [7] and food

processing [8]. Computational work on this topic is abundant in the literature. The first major studies of a steady two-dimensional lid-driven cavity flow are due to Burggraf [9] for a square cavity and by Pan and Acrivos [10] for other geometric aspect ratios. The results of a two-dimensional lid-driven cavity flow reported by Ghia et al. [11] and Schreiber and Keller [12] serve as classical benchmark data to validate results of several numerical solvers [13-16]. There also have been a number of studies on the flow in a three-dimensional lid-driven cavity [17-19]. Numerical benchmark data for a Reynolds number of 1000 in a cubic lid-driven cavity were reported by Albensoeder and Kuhlmann [20]. There are very few experimental studies in the literature on a lid-driven cavity flow. The first experiment was done by Koseff et al. [21-22] who used laser Doppler anemometer measurements on a three-dimensional lid-driven cavity with various aspect ratios. Particle image velocimetry (PIV) was used by Liberzon [23] to study the effects of dilute polymers and ethylene oxide in a lid-driven cavity in the turbulent regime. However, no combined numerical and experimental studies have been published on the mixing of miscible fluids in a lid-driven cavity. This, as well as its application in polymer mixing, are the reasons for investigating flow and mixing in such a relatively simple flow system.

Laser-based optical measurement techniques such as PIV and planar laser-induced fluorescence (PLIF) have been used in various processes to investigate single-phase flow, two miscible fluid flow and dilute two-phase flow [24]. As for the application of these optical measurement techniques on the mixing of two miscible fluids, it is necessary to achieve refractive index matching (RIM). If the refractive index difference is too large, the laser will be scattered at the uneven interface of the fluids, making it impossible to obtain accurate experimental data. To achieve a feasible environment for PIV and PLIF measurements, we selected two miscible fluids with almost the same refractive indices as working fluids in this work.

The aim of this paper is in the first place to show the feasibility of PIV and PLIF experiments in a lid-driven cavity with two miscible fluids, which is a simplified model of an industrial dynamic polymer mixer. In the second place, by comparing simulated flow fields and mixing process in the lid-driven cavity with the experimental data, we validate our simulation results and species transport models. In the third place, based on the verified simulation methods and models, we investigated the influences of density difference and viscosity of the two fluids on mixing performance. Based on this, we

propose a set of dimensionless parameters that characterize the mixing process in the cavity. We plan to quantify the mixing process based on these parameters in follow-up research.

The paper is organized as follows: in the next section, the experimental setup is discussed, including the flow system, PIV experiments, and PLIF experiments. Then, the numerical approaches we used in this research are briefly summarized with references. In the subsequent Results section, we first present the dynamic mixing process of the two miscible fluids starting from a layered state with the results of the PLIF experiments and simulations. Secondly, we compare the simulated velocity profiles with the PIV experimental data. Thirdly, we study the effects of density difference, viscosity and geometric scale-up on mixing performance in the lid-driven cavity by a dimensionless group $\frac{Ar}{Re}$ (the Archimedes number *Ar* and Reynolds number *Re* are defined in the next section) and identify the coefficient of variation (*COV*) to characterize the mixing efficiency. The final section summaries the main conclusions and suggests the future directions.

Experiments

Lid-driven cavity flow configuration

Fig. 2 shows the experimental setup including the lid-driven cavity (*L*x*W*x*H*=50x50x40 mm^3) made of Polymethyl methacrylate (PMMA) containing the two miscible liquids. A computer-controlled stepping motor (Shanghai ZHENGJI, China) drives the lid at a given speed *U*=0.02 m/s in *x* direction, and the fluctuations of the speed are within ± 1%. The experiments lasted 17.5 s as the maximum length of the lid in *x* direction was 400 mm. The time is non-dimensionalized as *Ut*/*L*.

Two kinds of sucrose solutions with little difference in mass fraction were used in the experiments, because their refractive indices match well. The properties of the two liquids are show in Table 1. The refractive indices of the liquids were measured with a WAY-2W Abbe refractometer (Shanghai INESA Instrument, China) and the dynamic viscosity with a MARS40 Rheometer (Haake, Germany). First, the cavity was filled with the dense Liquid 1 with a height of 0.75*H*, then it was filled with the light Liquid 2 with a height of 0.25*H*, as illustrated in Fig.2. In all the experiments, the Reynolds number $Re=\frac{\rho_1 UL}{\mu_1}$ (*L* the length of the cavity, ρ_1 the density of Liquid 1, μ_1 the viscosity of Liquid 1) is 12.68. The Archimedes number is defined as $Ar=\frac{gL^3\rho_1(\rho_1-\rho_2)}{\mu_1^2}$ (*g* is gravitational acceleration) to investigate the effects of density difference

on the mixing process of the two miscible fluids. Another dimensionless number (Schmidt number) $Sc_i = \frac{\mu_i}{\rho D_m}$ is also considered as an important variable that affects the mixing performance of miscible fluids, and μ_i is the viscosity of Liquid 1 or Liquid 2. D_m is the mass diffusion coefficient between Liquid 1 and Liquid 2. The self-diffusive coefficient of a 61.5 wt.% sucrose solution is about 1.5×10^{-10} m^2/s as measured by Irani and Adamson [25], which leads to *Sc* reaching a value of the order of 10^5 for Liquid 1 as well as Liquid 2. When *Sc* is larger than 10^4, the mixing behavior is totally dominated by fluid convection at low Reynolds numbers ($Re \leq 40$) [26-27]. Therefore, the effect of mass diffusion on the mixing performance is expected to be negligible in this experiment.

PIV Measurement Technique

The 2D-PIV system used in this work is a commercial system from Dantec (Denmark). It consists of a laser (Dual power, 532 nm, 100 mJ, 100 Hz), spherical and cylindrical lenses which transform the laser beam into a laser sheet with thickness of 1 mm in the measurement plane, a CMOS camera (SpeedSense 4 MP, 2320 x 1720 pixel, 193Hz), a synchronizer, and dynamic studio software. Hollow spherical glass particles (TSI, USA) with diameters of about 8-12 μm and density of 1500 kg/m^3 were used as tracer particles.

The (*x*, *y*, *z*) coordinate system is shown in Fig. 2. The velocities in the three Cartesian directions (*x*, *y*, *z*) are represented by *u*, *v*, and *w* respectively. As shown in Fig. 2, the origin of the coordinate system is the left bottom corner in the *x*-*z* plane that crosses the center of the cavity. The PIV measurement region was the entire *y*=0 plane (*L*x*H*=50x40 mm^2). The PIV images were analyzed by using dynamic studio software (Dantec Inc). An adaptive interrogation windows method was used, in which the size and shape of the individual interrogation areas can be iteratively adjusted to adapt to local seeding densities and flow gradients [28-29]. The minimum size of the interrogation windows was 32 × 32 $pixels^2$, and the grid step size was 16 × 16 $pixels^2$. The image resolution was 26.67 μm/pixel, thus the velocity vector resolution was one vector per 0.43 mm. The frame rate of the camera was such that 70 vector fields per second were measured.

The camera captured the whole mixing process; it started capturing before the lid started and ended capturing after the lid had stopped. The time interval between the two laser pulses – that together generate a single PIV velocity vector field – Δt was determined as 6000 μs to ensure that the maximum in-plane and out-of-plane displacements of the tracer

particles were less than one-quarter of the interrogation windows size and of the thickness of the laser sheet.

PLIF Measurement Technique

We refer to Fig. 2 for explaining the PLIF experiment on mixing in the lid-driven cavity. Liquid 1 in the cavity did not contain Rhodamine B. Rhodamine B was uniformly dispersed in Liquid 2, and Liquid 2 was carefully placed on top of Liquid 1. The concentration of Rhodamine B in Liquid 2 was 50 μg/L and it was confirmed that it had – within experimental accuracy – no influence on the physical properties of Liquid 2. Fluorescence of the molecules of Rhodamine B is induced by the green band of the laser (λ=532 nm). Its absorption maximum occurs in the vicinity of 540 nm and its fluorescence maximum occurs around 590 nm [30]. The excited fluorescence intensity was captured by the CMOS camera equipped with a sharp cut-off filter blocking out any incident scattered light with a wavelength below 550 nm [31].

Calibration is a vitally important step of PLIF experiments. It is performed by measuring homogeneous solutions with known concentrations. The tracer is excited and emits fluorescence with a specific wavelength when the laser sheet passes through a liquid containing Rhodamine B. There is a functional relationship between the amount of emitted fluorescence captured by the CMOS camera and the concentration of Rhodamine B. The relationship between the intensity of excited fluorescence and the concentration of tracer can be given as [32-34]:

$$I = \Gamma_1 C \cdot exp\,(-\Gamma_2 C) \qquad (1)$$

$$I_c = I + I_b \qquad (2)$$

where *I* is the fluorescence intensity, *C* is the tracer concentration, Γ_1 is a local coefficient related to the experimental parameters, Γ_2 is a coefficient that takes into account the effect of absorption, I_c is the light intensity captured by the CMOS camera, and I_b is the intensity of background. It can be seen from Eq. (1) that the fluorescence intensity is linearly proportional to the local tracer concentration at low excitation intensity. At high excitation, there is no longer a linear relationship between the fluorescence intensity and the concentration of tracer due to saturation and photo bleaching effects [32].

In this work, a series of measurements for calibration was performed at several tracer concentrations in homogeneous Liquid 1 and Liquid 2. Fig. 3 shows the relationship between the fluorescence intensity and the tracer

concentration in the two liquids. It can be seen that the relationship is to a very good approximation linear if the concentration is in the range 0 - 60 μg/L. Therefore, the initial tracer concentration in our experiments was chosen at 50 μg/L to ensure a linear relationship between the measured light intensity and the Rhodamine B concentration. The fluorescence intensity of Liquid 1 and Liquid 2 for any given concentration in the range 0 – 60 μg/L differs by less than 3% (see Figure 3). This thus allows us to accurately measure the composition of this miscible liquid system through measuring the Rhodamine B concentration. Based on the linear relationship in Fig. 3, the gray-level images captured by the CMOS camera were converted to concentration profiles of the Rhodamine B which is proportional to the concentration of Liquid 2. For a better view of the concentration field obtained in the PLIF measurements, the gray-level images were converted to pseudo-color images by a Matlab code, as shown in Fig. 4. In the pseudo-color images, blue region with a RGB value of [0, 0, 255] is considered as the region with 0 vol.% of Liquid 2, and red region with [255, 0,0] is the region with 100 vol.% of Liquid 2.

Simulations

Species transport model

Simulations on flows of multi-component Newtonian fluids are based on the solution of the continuity and Navier-Stokes equations. They have the following form:

$$\frac{\partial \rho}{\partial t} + \nabla \cdot \left(\rho \vec{u} \right) = 0 \tag{3}$$

$$\frac{\partial \rho \vec{u}}{\partial t} + \nabla \cdot \left(\rho \vec{u} \vec{u} \right) = -\nabla p + \nabla \cdot \left(\mu \nabla \vec{u} \right) + \rho \vec{g} \tag{4}$$

where ρ is the fluid density, p is the pressure, $\vec{u}$ is the velocity, and μ is the viscosity, $\vec{g}$ is the gravitational acceleration.

A species transport model was employed for simulating the mixing process of the two miscible fluids in the lid-driven cavity. The conservation of species i can be given as follows [35]:

$$\frac{\partial \left(\rho f_i \right)}{\partial t} + \nabla \cdot \left(\rho f_i \vec{u} \right) = \nabla \cdot \left(\rho D_m \nabla f_i \right) \tag{5}$$

where f_i is the local mass fraction of the species i, and D_m is the mass diffusion coefficient. An equation of this form will be solved for $N-1$ species with N the total number of fluid species presented in the system. Since the mass fraction of the

species must sum to unity, the N_{th} mass fraction is determined as one minus the sum of the N-1 solved mass fractions. To minimize numerical error, the N_{th} species should be selected as the species with overall largest mass fraction. In this work, the conservation equation of Liquid 2 was solved and the mass fraction of Liquid 1 was determined as one minus the mass fraction of Liquid 2.

The effective viscosity of the mixture is determined through the mass fraction and the viscosity of each Liquid:

$$\mu = f_1 \mu_1 + (1 - f_1) \mu_2 \quad (6)$$

where f_1 is the mass fraction of Liquid 1, and μ_1 and μ_2 are the viscosities of Liquid 1 and 2 respectively.

The density of the mixture is expressed in terms of the mass fraction and the density of each liquid in the following way:

$$\frac{1}{\rho} = \frac{f_1}{\rho_1} + \frac{(1 - f_1)}{\rho_2} \quad (7)$$

where ρ_1 and ρ_2 are the densities of Liquid 1 and Liquid 2 respectively.

Eq. (6) and Eq. (7) were compiled in Fluent 18.0 [36] by external user-defined functions. As shown in the experiments section, the concentration is described in terms of volume fraction, so f_1 is translated to C_1 by $C_1 = f_1 \frac{\rho}{\rho_1}$.

Numerical details

No turbulence model (direct simulation) was used to calculate the flow field in the lid-driven cavity because the largest Reynolds number of all simulation cases was 486. The species transport model was selected to realize the mixing of two miscible fluids. In all the simulations, D_m was chosen as 1.5×10^{-10} m^2/s which has been discussed in the experiments section.

The geometric configuration used for the CFD simulations in this work was the same as that used for the PIV experiments. The geometry and the mesh were constructed by using a commercial software ICEM [37]. Hexahedral elements (about 3.2 million with grid spacing Δx of about 0.31 mm) were used for meshing the geometry. A grid sensitivity study has been carried out and the results will be explained later. The lid of the cavity was set as a moving wall boundary with a given speed U of 0.02 m/s in positive x direction. No-slip condition was applied to all solid wall boundaries. As for the temporal resolution, time step Δt was set as 0.005 s to keep the Courant-Friedrichs-Levy number ($\frac{U \Delta t}{\Delta x}$)

smaller than 1 according to ANSYS Fluent Users guide [38]. The second order upwind scheme was used for the spatial discretization of the momentum equations, and the second-order implicit scheme for time advancement. In order to couple pressure and velocity, the SIMPLE (Semi-Implicit Method for Pressure Linked Equations) algorithm was used. Convergence per time step was achieved when the normalized residuals of the continuity and velocities became less than 10^{-4} and the normalized residuals of the mass fraction became less than 10^{-7}.

Results and Discussion

Mixing progress in the lid-driven cavity flow

Fig. 5a shows the mixing process of the lid-driven cavity flow visualized by the PLIF measurements. At Ut/L=0, two liquids are layered up and down with a clear interface. With the movement of the lid, Liquid 2 begins moving to the right part of the cavity and Liquid 1 fills the region previously occupied by the Liquid 2. Because of the confinement by the right sidewall, the nearby Liquid 2 moves downwards. At Ut/L=3, Liquid 2 is drawn down into Liquid 1, and Liquid 2 is not in direct contact with the lid anymore. At this moment, the Liquid 1 driven by the lid reaches the right sidewall, and then moves downward. More and more Liquid 1 is carried by the moving lid and then moves around the main region of the Liquid 2, as shown from Ut/L=3 to Ut/L=6 in Fig. 5a. In this process Liquid 1 gradually cuts Liquid 2 into a large triangular region and a narrow striation at Ut/L=7. Because of the restriction of the lid length in x direction, the mixing process after Ut/L=7 cannot be obtained in the experiments. We used numerical simulations to predict the two liquid mixing beyond Ut/L=7.

The simulated results regarding the above-mentioned mixing process are presented in Fig. 5b. The predicted mixing process from lid starting to the moment Ut/L=7, including carrying Liquid 1 by the lid, separating the Liquid 2 into a triangular region and striations, is in good agreement with the experimental results. In the simulation, we extended the mixing process to the moment Ut/L=16. As the lid continuous moving, the circulation of the Liquid 1 promotes the mixing with the Liquid 2 in the triangular region, and the area of the region becomes smaller from Ut/L=7 to Ut/L=16. The striation of Liquid 2 is gradually disappearing at Ut/L=16. The formation of the stable triangular region of the Liquid 2 might be caused by the low operating Reynolds number; only limited mixing happens over a short time period at

Re=12.68.

Concentration profiles of the Liquid 2 at *Ut*/*L*=3 and *Ut*/*L*=7 on a horizontal line *z*/*H*=0.75 and a vertical line *x*/*T*=0.85 are shown in Fig. 6 for a quantitative comparison. The predicted concentration profiles of Liquid 2 at *z*/*H*=0.75 agree well with the experimental data at the two moments, although the concentration of the Liquid 2 in the striation is overpredicted at *Ut*/*L*=7. On the vertical line *x*/*T*=0.85, the simulated width of the triangular region and the striations is smaller than the experimental data. Simulated concentration distributions of Liquid 2 at *Ut*/*L*=7 with different grids are shown in Fig. 6. The concentration contour with 3.2 million cells is not displayed in Fig. 6 as it is already presented in Fig. 5(b). Good agreement in terms of simulated concentration fields are obtained by using the three grids, but the results are to some extent grid dependent. As the Schmidt number in the simulations is of the order of 10^5, fine concentration length scales will develop that can be captured better on finer grids. This is noticeable in the quantitative comparisons at *z*/*H*=0.75 and *x*/*T*=0.85 in Fig. 6(b). As a compromise between numerical accuracy and computational efficiency, most simulated results in this work are based on the grid with 3.2 million cells. The effect of grid on the simulated results will be further discussed in the following sections.

In general, the simulated results of volume concentration can give a good prediction of the mixing of the two miscible fluids. From these visualizations, it is demonstrated that the PLIF experiments as well as the related simulations can effectively describe the mixing process of the two miscible fluids in the lid-driven cavity. In the next section, the results of the PLIF experiments will be combined with the velocity field obtained by the PIV measurements to interpret these phenomena in more detail.

Flow Fields in the lid-driven cavity

The PIV measurements were conducted under the same operating conditions as the PLIF experiments, however not simultaneously with the PLIF experiments. The experimental flow fields at four moments are shown in the left column of Fig. 7. To explore the connection between the velocity fields and the concentration fields, we show the outline of Liquid 2 (by marking the contour where volume fraction of Liquid 2 is equal to 0.9 as a red curve) in Fig. 7. At *Ut*/*L*=1, a small flat cycle flow pattern is formed and the region with a velocity magnitude of 0.2*U* and higher is very small. Within a short time

period, the entire Liquid 2 is just carried by the lid to the right side of the cavity and the main circulation has not yet formed. With the continuous movement of the lid, a single-cycle flow pattern was formed at Ut/L=3. The contour of the flow field is strongly asymmetric and the center of the single-cycle pattern is offset to the right wall at about x/L=0.7. From Ut/L=3 to Ut/L=7, there is no significant change for the center of the single-cycle pattern so that the main part of Liquid 2 keeps in a large triangular region with some striations. There are, however, some small changes in the magnitudes of the velocity around the triangular region. The simulated instantaneous realizations of velocity fields in the lid-driven cavity with two miscible fluids are shown in the right column of Fig. 7. There is also a small flat cycle flow pattern at Ut/L=1, and the single-cycle pattern with the center at x/L=0.7 is formed at Ut/L=3. From Ut/L=3 to Ut/L=7, the magnitudes of the simulated velocity around the triangular region keep changing as in the experiments.

As shown in Fig. 8, u and w on two horizontal lines (z/H=0.75 and z/H=0.95) and two vertical lines (x/L=0.50 and x/L=0.95) at Ut/L=7 are chosen to present the quantitative comparisons between experimental and simulated results in terms of fluid velocity. Although there are some discrepancies, the simulated results are in good agreement with experimental data, which gives us confidence that we can use simulations for predicting the mixing process of two miscible fluids under a laminar condition. The profiles show that our simulated velocity results with 3.2 million cells is already grid insensitive, because the results of 6.4 million cells overlap with those of 3.2 million cells in Fig. 8.

The flow fields in the lid-driven cavity with two miscible fluids show clear distinctions with the flow fields with only one fluid [17]. To investigate the differences and verify the simulation method again, a PIV experiment for the cavity only filled with Liquid 1 was conducted. The instantaneous PIV results in the cavity with one fluid are shown in the left column of Fig. 9. Comparing the velocity fields at the four moments, we can find that the single-cycle flow pattern has been preliminarily formed at Ut/L=1. With the continuous drag of the lid, the overall flow field in the cavity has not changed much after Ut/L=3. In general, the contours of the flow fields in the cavity with only one fluid is relatively symmetrical compared with the flow field with two miscible fluids. The center of the single-cycle in the cavity with only one fluid is located at about x/L=0.5, which is similar to the results in the literature [13]. In addition, the region with velocity magnitude of at least 0.2U extends to z/H=0.25 which is significantly deeper than that in the cavity with two fluids at

Ut/*L*=5. Impressions of the simulated instantaneous velocity field in the cavity with one fluid over time are given in the right column of Fig. 9. Both the single-cycle flow pattern and the area reaching the speed of 0.2*U* can be well predicted by the simulations.

To quantify the results of the experiments and simulations, we present the *u* and *w* velocity profiles on two horizontal lines (*z*/*H*=0.75 and *z*/*H*=0.95) and two vertical lines (*x*/*L*=0.50 and *x*/*L*=0.95) at *Ut*/*L*=7 in Fig. 10. In general, simulations and experiments in the lid-driven cavity with one fluid are in good agreements. The velocity profiles in Fig. 10 also confirm that our simulated velocity fields with 3.2 million cells is already grid insensitive. Compared with the grid effects on the mixing process in previous section, it is much easier to achieve a grid independent flow field.

In summary, simulations can well predict the flow fields in the cavity with one or two kinds of miscible fluids. The flow fields in the cavity with two miscible fluids show clear distinctions with those with only one fluid. The buoyancy caused by the small density difference plays an important role in the flow and mixing process. Because of experimental limitations, such as refractive index matching among fluids with density difference, the effect of density difference and viscosity on the mixing performance could not be experimentally investigated over a wide range of parameters. In the next section, many groups of simulations will be conducted to find the parameters most influencing the mixing performance.

Effect of $\frac{Ar}{Re}$ on mixing performance

The influence factors on the mixing process will be discussed based on simulations in this section. A different density difference of the two fluids will bring about different buoyancy, and changes in viscosity cannot be ignored due to the small Reynolds numbers in this study. Thus, a dimensionless group $\frac{Ar}{Re} \equiv \frac{(\rho_1 - \rho_2)gL^2}{\mu U}$ is defined as the ratio of buoyancy ($(\rho_1 - \rho_2)gL^3$) to viscous force ($\mu \frac{U}{L} L^2$).

To quantify the mixing efficiency of the two miscible fluids in the lid-driven cavity flow, coefficient of variation (*COV*) was calculated to represent the standard deviation of liquid concentration [39]:

$$COV = \frac{\left(\iint_A \left(C_{\text{avg}} - C \right)^2 \, dA \right)^{0.5}}{C_{\text{avg}}} \tag{8}$$

$$C_{\text{avg}} = \frac{1}{A} \iint_A C_l \, dA \tag{9}$$

where C_{avg} is average scalar concentration over a selected plane and A is the area of the plane (m^2).

A more complex operating condition with small $\frac{Ar}{Re}$ of 0 and large Ut/L of 16 was selected to specify the effect of the grid on the mixing process. The simulated concentration of Liquid 2 in the cavity at Ut/L=16 with 1.6, 3.2 and 6.4 million is shown in the top row of Fig. 11, and concentration profiles of the Liquid 2 at Ut/L=16 on a horizontal line z/H=0.75 are shown in the left bottom of Fig. 11. Time series of *COV* at $\frac{Ar}{Re}$=0 are bottom-right in Fig. 11. We observe a clear grid dependence. With a Schmidt number of 10^5 it will not be possible to achieve grid convergence for the scalar concentration field. The scalar diffusion distance δ over the time for one lid passage (L/U) is $\delta/L=(ScRe)^{-1/2}\approx 0.0004$. We thus would need a grid with of the order of $(L/\delta)^3 \approx 1.5\text{x}10^{10}$ control volumes to capture the concentration field in full detail which is computationally unfeasible. For practical reasons, subsequent simulations for identifying trends in scalar mixing are all based on grids with 3.2 million cells and we realize that at this level of resolution, grid convergence for the concentration field has not yet been reached.

To investigate the effect of density difference, a constant viscosity 0.103 Pa·s was chosen for the two fluids. The density of Liquid 1 was kept as 1307 kg/m^3, and the density of Liquid 2 was changed from 1307 to 1241.65 kg/m^3, resulting in density difference ranging from 0 to 65.35 kg/m^3 and $\frac{Ar}{Re}$ from 0 to 778. Instantaneous concentration distribution at four $\frac{Ar}{Re}$ are shown in Fig. 12. At high $\frac{Ar}{Re}$ of 778, the upper fluid cannot be dragged into the lower one. When $\frac{Ar}{Re}$ is 119, the main part of the Liquid 2 forms a stable triangular region from Ut/L=8 to Ut/L=16. Further decreasing $\frac{Ar}{Re}$ to 31, a noticeable mixing process can be seen with thin striations continuously being separated from the main part of Liquid 2. When $\frac{Ar}{Re}$ is 0, more striations are generated within Ut/L=16 and then are dissipated in the entire cavity. The shape of the main part of Liquid 2 changes a lot and its area becomes smallest in comparison with other three cases. It is obvious that mixing performance becomes better with decreasing $\frac{Ar}{Re}$ (as a result of small density difference).

Time series of *COV* at four $\frac{Ar}{Re}$ are plotted in Fig. 13. At constant $\frac{Ar}{Re}$, the *COV* value decreases with the increase of time, that is, the level of mixing improves with time. The *COV* decreases very slowly at $\frac{Ar}{Re}$ = 778 as mixing only occurs at the interface of the two liquids, and the *COV* value at $\frac{Ar}{Re}$ = 119 does hardly decrease for Ut/L>12 because the main part of the Liquid 2 forms a stable triangular region, as shown in Fig. 12. At constant Ut/L, the lower the $\frac{Ar}{Re}$, the smaller the

COV value, and thus the better the liquid mixing. Best mixing performance occurs at $\frac{Ar}{Re}$=0, and minimizing the density difference of the two fluids is recommended as a way to achieve faster mixing.

In Fig.14, fluids with the same densities as those in the experimental configurations (ρ_1=1307 kg/m^3, ρ_2=1297 kg/m^3) are used to investigate the effects of viscosity on the mixing performance. The number $\frac{Ar}{Re}$ ranges from 11900 to 1.19 due to the viscosities (μ_1=μ_2) ranging from 0.00103 to 10.3 Pa·s. At the highest $\frac{Ar}{Re}$ of 11900 (as a result of the lowest viscosity), mixing happens within a narrow region between the main parts of the two fluids, and the interface at z/H=0.75 has not changed much at Ut/L=16. With the decrease of $\frac{Ar}{Re}$, more Liquid 2 is separated by the Liquid 1, forming different striation structures, and then better mixing is achieved. In general, viscous effects enhance the mixing of the two miscible fluids in the lid-driven cavity.

Four pairs of simulations with various density difference and viscosity but the same $\frac{Ar}{Re}$ were conducted, and the parameters of the cases are shown in Table 2. Simulated concentrations and quantitative comparisons of Liquid 2 at Ut/L=16 are shown in Fig. 15. By comparing the first two column of Fig. 15, we observe that cases with constant $\frac{Ar}{Re}$ present almost the same mixing performance when $\frac{Ar}{Re}$ ≤119. A quantitative comparison of the Liquid 2 concentration at a horizontal line z/H=0.75 (see the right column of Fig. 14) further confirms this conclusion.

However, curved interface between the two liquids can be found when $\frac{Ar}{Re}$ is 1190, as shown in the middle panel of the first row in Fig. 15. The main reason might be that the flow in the cavity is not laminar as the Reynolds number is 486 for this case. Time series of *COV* were presented in Fig. 16. The *COV* decreases very slowly at $\frac{Ar}{Re}$ = 1190 because the concentration profiles only undergo minor changes over time and Liquid 2 is not entrained in Liquid 1 and does not form striations, as shown in Fig. 15. The simulated cases with constant $\frac{Ar}{Re}$ show almost the same mixing process including the case with $\frac{Ar}{Re}$=1190, and better mixing performance can be achieved with a small $\frac{Ar}{Re}$.

To confirm the $\frac{Ar}{Re}$ scaling, three cases with different U and L but constant $\frac{Ar}{Re}$ were simulated. The concentration field of Liquid 2 of the three cases at Ut/L=16 are shown in the left three panels of Fig. 17. The three concentration fields are almost the same in terms of the contours shown in Fig. 17. To quantitatively compare the results of the three cases, we present concentration profiles on a horizontal line z/H=0.75 at Ut/L=16 in the right panel of Fig. 17. The almost overlapping

concentration profiles confirm that cases with constant $\frac{Ar}{Re}$ value will lead to the same mixing performance and concentration distribution.

Conclusion and Future work

A simplified model based on an industrial dynamic mixer was realized by a lid-driven cavity flow with two miscible fluids. Refractive index matching between the two fluids was achieved to visualize the mixing process in the cavity. Instantaneous concentration and velocity fields were measured by using the PLIF and 2D-PIV experiments respectively. The mixing characteristics are closely associated with the flow field of the two fluids, which is quite different from the flow field in the cavity with only one fluid. To the best of our knowledge, this is the first work about visualizing the mixing and flow field of two miscible fluids in a cavity flow by using PIV and PLIF experiments.

Instantaneous concentration distribution and velocity field were predicted by the CFD simulations with species transport models. The simulated results are quantitatively verified by the experimental data, and they agree very well with each other. The present work gives us confidence to simulate the mixing process in industrial dynamic mixers, such as the configuration shown in Figure 1.

A dimensional group $\frac{Ar}{Re}$ is proposed to investigate the effect of fluids properties such as density difference and viscosity and of geometric and operation parameters including lid velocity and cavity size. The mixing performance in terms of the *COV* of fluid concentration becomes better with the decrease of $\frac{Ar}{Re}$. At constant $\frac{Ar}{Re}$ in the range of $1.19 \leq \frac{Ar}{Re} \leq 119$, we can obtain approximately the same mixing process by changing the fluids properties, geometric and operation parameters. For the design and optimization of dynamic mixers involving laminar flow with density differences, this paper has identified the dimensionless group $\frac{Ar}{Re}$ as an important design parameter.

This work investigated the mixing characteristics in a laminar lid-driven cavity based on simplifying an industrial dynamic mixer. The validated computational methods and models could be used to simulate industrial dynamic mixers in the future. However, grid effects on the concentration field are hard to avoid due to the high Schmidt number. The mixing process of miscible non-Newtonian fluids with a wide range of Reynolds numbers in lid-driven cavities as well as in dynamic mixers will also be our future research directions.

Acknowledgement

The authors gratefully acknowledge the financial support from the National and Key Research and Development Program of China (No.2016YFB0302801), National Natural Science Foundation of China (No.21676007) and Scientific Research and Technology Development Projects of China National Petroleum Corporation (No. 2016B-2605).

References

[1] R.S. Hindmarch, The cavity transfer mixer: a blender for all seasonings, Mater. Des. 8 (1987) 331–339.
[2] Z. Jiang, Z. Guo, Z. Jia, J. Wang, C. Pu, C. Xiao, J. Jin, Mixing mechanism and evaluation of the dispersion effect of a 3D dynamic Mixer, J. Test. Eval. 44 (2016) 367-375.
[3] C. Wang, I. Manas-Zloczower, Flow field analysis of a cavity transfer mixer, Polym. Eng. Sci. 34 (1994) 1224–1230.
[4] A.A. Woering, W.C.M. Gorissen, A. Biesheuvel, Optimization of viscous mixing in a two-dimensional cavity transfer mixer, Flow. Turbul. Combust. 60 (1998) 377–407.
[5] G. Grosso, M.A. Hulsen, A. S. Fard, P.D. Anderson, A. Overend, Mixing processes in the cavity transfer mixer: a thorough study, AIChE J. 64 (2018) 1034–1048.
[6] C.B. Shin, Forced and natural convection effects on the shape evolution of cavities during wet chemical etching, J. Electrochem. Soc. 138 (1991) 527-538.
[7] J.B. Ritz, F. Bertrand, F. Thibault, P.A. Tanguy, Shear-induced particle migration in a short-dwell coater, Chem. Eng. Sci. 55 (2000) 4857–4867.
[8] S. Bruin, D.J.V. Zuilichen, W. Stolp, A review of fundamental and engineering aspects of extrusion of biopolymers in a single-screw extruder, J. Food Process Eng. 2 (1978) 1–37.
[9] O.R. Burggraf, Analytical and numerical studies of the structure of steady separated flows, J. Fluid Mech. 24 (1966) 113–151.
[10] F. Pan, A. Acrivos, Steady flows in rectangular cavities, J. Fluid Mech. 28 (1967) 643–655.
[11] U. Ghia, K.N. Ghia, C.T. Shin, High-Re solutions for incompressible flow using the navier-stokes equations and a multigrid method, J. Comput. Phys. 48 (1982) 387–411.
[12] R. Schreiber, H.B. Keller, Driven cavity flows by efficient numerical techniques, J. Comput. Phys. 49 (1983) 310–333.
[13] S. Thakur, W. Shyy, H.S. Udaykumar, L. Hill, Multiblock interface treaments in a pressure-based flow solver, Numer. Heat Transf, Part B. 33 (1998) 367–396.
[14] A.T. Degani, G.C. Fox, Parallel multigrid computation of the unsteady incompressible navier-stokes equations, J. Comput. Phys. 128 (1996) 223–236.
[15] T.W.H. Sheu, Y.X. Lin, C.H. Yu, Numerical study of two regularization models for simulating the turbulent flows, Comput. Fluids. 74 (2013) 13–31.
[16] D.A. Shetty, T.C. Fisher, A.R. Chunekar, S.H. Frankel, High-order incompressible large-eddy simulation of fully inhomogeneous turbulent flows, J. Comput. Phys. 229 (2010) 8802–8822.
[17] K.M. Akyuzlu, J. Farkas, A study of formation of circulation patterns in laminar unsteady lid-driven cavity flows using PIV measurement techniques, ASME 2012 International Mechanical Engineering Congress and Exposition. 7 (2012) 1221-1230.
[20] K. Anupindi, W. Lai, S. Frankel, Characterization of oscillatory instability in lid driven cavity flows using lattice boltzmann method, Comput. Fluids. 92 (2014) 7–21.
[19] L.Q. Tang, T. Cheng, T.T.H. Tsang, Transient solutions for three-dimensional lid-driven cavity flows by a least-squares finite element method, Int. J. Numer. Methods Fluids. 21 (1995) 413–432.
[20] S. Albensoeder, H.C. Kuhlmann, Accurate three-dimensional lid-driven cavity flow, J. Comput. Phys. 206 (2005) 536–558.
[21] A.K. Prasad, J.R. Koseff, Reynolds number and end-wall effects on a lid-driven cavity flow, Phys. Fluids A. 1 (1989) 208–218.
[22] J.R. Koseff, R.L. Street, The lid-driven cavity flow: a synthesis of qualitative and quantitative observations, J. Fluids Eng. 106 (1984) 385-389.
[23] A. Liberzon, On the effects of dilute polymers on driven cavity turbulent flows, Int. J. Heat Fluid Flow. 32 (2011) 1129–1137.
[24] S.F. Wright, I. Zadrazil, C.N. Markides. A review of solid–fluid selection options for optical-based measurements in

single-phase liquid, two-phase liquid–liquid and multiphase solid–liquid flows. Exp. Fluids. 58 (2017) 108.
[25] R.R. Irani, A.W. Adamson, Transport processes in binary liquid systems, J. Phys. Chem. 62 (1958) 1517–1521.
[26] V. Kumar, M. Aggarwal, K.D.P. Nigam, Mixing in curved tubes, Chem. Eng. Sci. 61 (2006) 5742–5753.
[27] M. Mansour, Z. Liu, G. Janiga, K.D.P. Nigam, K. Sundmacher, D. Thévenin, K. Zähringer, Numerical study of liquid-liquid mixing in helical pipes, Chem. Eng. Sci. 172 (2017) 250–261.
[28] Y. Zhang, Z. Gao, Z. Li, J.J. Derksen, Transitional flow in a rushton turbine stirred tank, AIChE J. 63 (2017) 3610–3623.
[29] R. Theunissen, F. Scarano, M.L. Riethmuller, An adaptive sampling and windowing interrogation method in PIV, Meas. Sci. Technol. 18 (2007) 275–287.
[30] P.E. Arratia, F.J. Muzzio, Planar laser-induced fluorescence method for analysis of mixing in laminar flows, Ind. Eng. Chem. Res. 43 (2004) 6557–6568.
[31] D.R. Unger, F.J. Muzzio, Laser-induced fluorescence technique for the quantification of mixing in impinging jets, AIChE J. 45 (1999) 2477–2486.
[32] I. Houcine, H. Vivier, E. Plasari, R. David, J. Villermaux, Planar laser induced fluorescence technique for measurements of concentration fields in continuous stirred tank reactors, Exp Fluids. 22 (1996) 95–102.
[33] F. Guillard, R. Fritzon, J. Revstedt, C. Tragasrdh, M. Alden, L. Fuchs, Mixing in a confined turbulent impinging jet using planar laser-induced fluorescence, Exp. Fluids. 25 (1998) 143–150.
[34] P. Luo, Y. Cheng, Z. Wang, Y. Jin, W. Yang, Study on the mixing behavior of thin liquid-sheet impinging jets using the PLIF technique, Ind. Eng. Chem. Res. 45 (2006) 863–870.
[35] S.K. Dahikar, J.B. Joshi, M.S. Shah, A.S. Kalsi, C.S. RamaPrasad, D.S. Shukla, Experimental and computational fluid dynamic study of reacting gas jet in liquid: flow pattern and heat transfer, Chem. Eng. Sci. 65 (2010) 827–849.
[36] ANSYS Fluent UDF Manual, ANSYS Inc. 2017.
[37] ANSYS ICEM CFD Help Manual, ANSYS Inc. 2017.
[38] ANSYS Fluent User Guide, ANSYS Inc. 2017.
[39] M.M. Mandal, P. Aggarwal, K.D.P. Nigam, Liquid-liquid mixing in coiled flow inverter, Ind. Eng. Chem. Res. 50 (2011) 13230–13235.

Table 1

Table 1 Properties of two miscible liquids

	sucrose aqueous solution	Density (kg/m^3)	viscosity at 20°C (Pa·s)	refractive index at 20°C	liquid height
Liquid 1	63.0wt% sucrose	1307	0.103	1.4486	0.75*H*
Liquid 2	61.5wt% sucrose	1297	0.079	1.4460	0.25*H*

Table 2

Table 2 Parameters of four pairs with same value of $\frac{Ar}{Re}$

Pair	*Ar*/*Re*	density difference (kg/m^3)	viscosity (Pa·s)
1	1.19	10	10.3
	1.19	2.614	2.692
2	11.9	10	1.03
	11.9	2.614	0.2692
3	119	10	0.103
	119	2.614	0.02692
4	1190	10	0.0103
	1190	2.614	0.002692

Figure 1

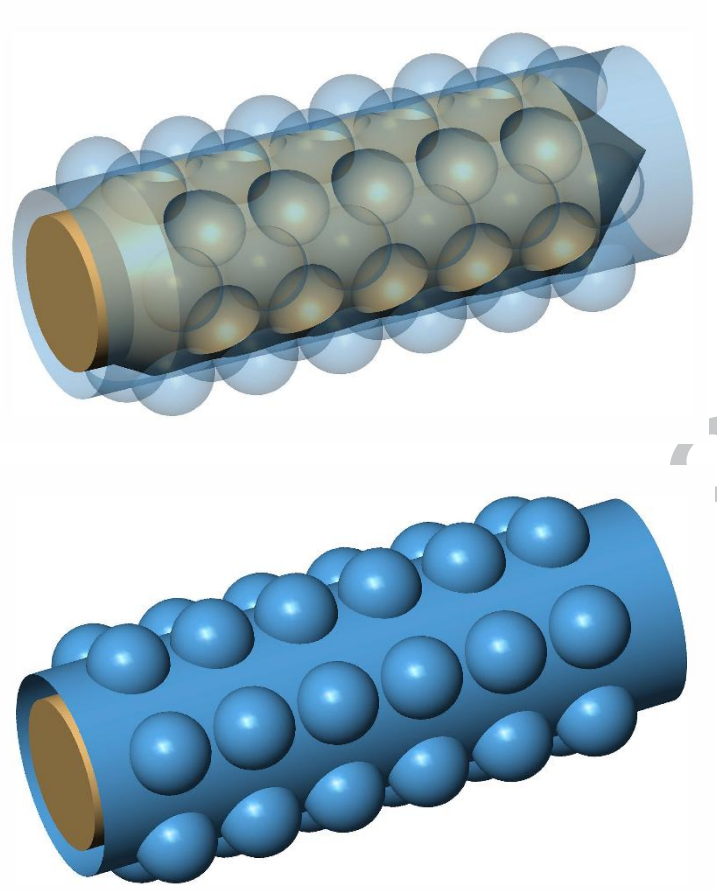

Fig. 1. Geometry of a dynamic mixer with an inner rotating part (see the top panel) and an outer stationary part (see the bottom panel). Cavities in the rotating part partly overlap with those in the stationary part. During operation, two materials flow through the mixer from the left to the right side, being mixed by the cavities.

Figure 2

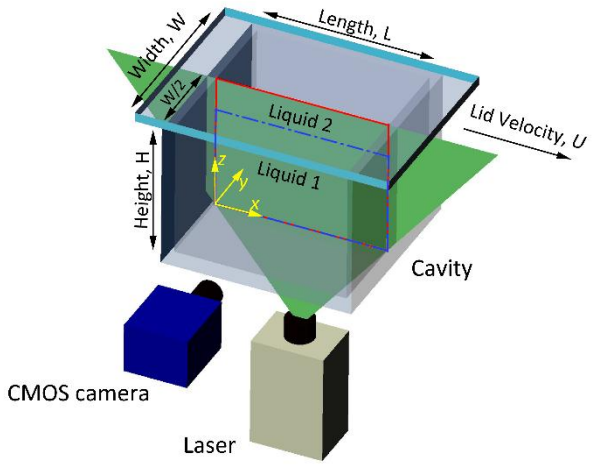

Fig. 2. Schematic experimental setup, parameters of the cavity, the coordinate system, and the measurement region shown by the red rectangle. The lid (the top wall) moved in *x* direction with a velocity *U*. Before the lid started moving, the heavier Liquid 1 was below the lighter Liquid 2 with a clear and horizontal interface.

Figure 3

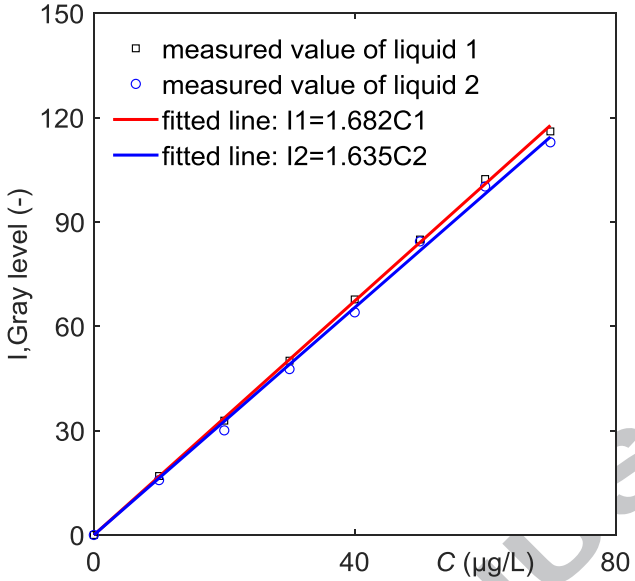

Fig. 3. The fluorescence intensity of Rhodamine B tracer (gray level of the captured images) as a function of the tracer concentration in Liquid 1 and Liquid 2.

Figure 4

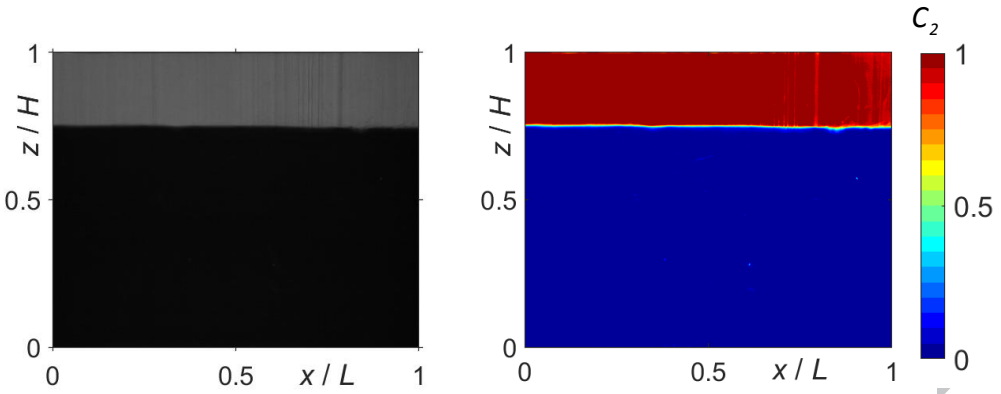

Fig. 4. Left panel: raw gray-level image before the lid started moving. Right panel: concentration distribution of Liquid 2 after image processing.

Figure 5

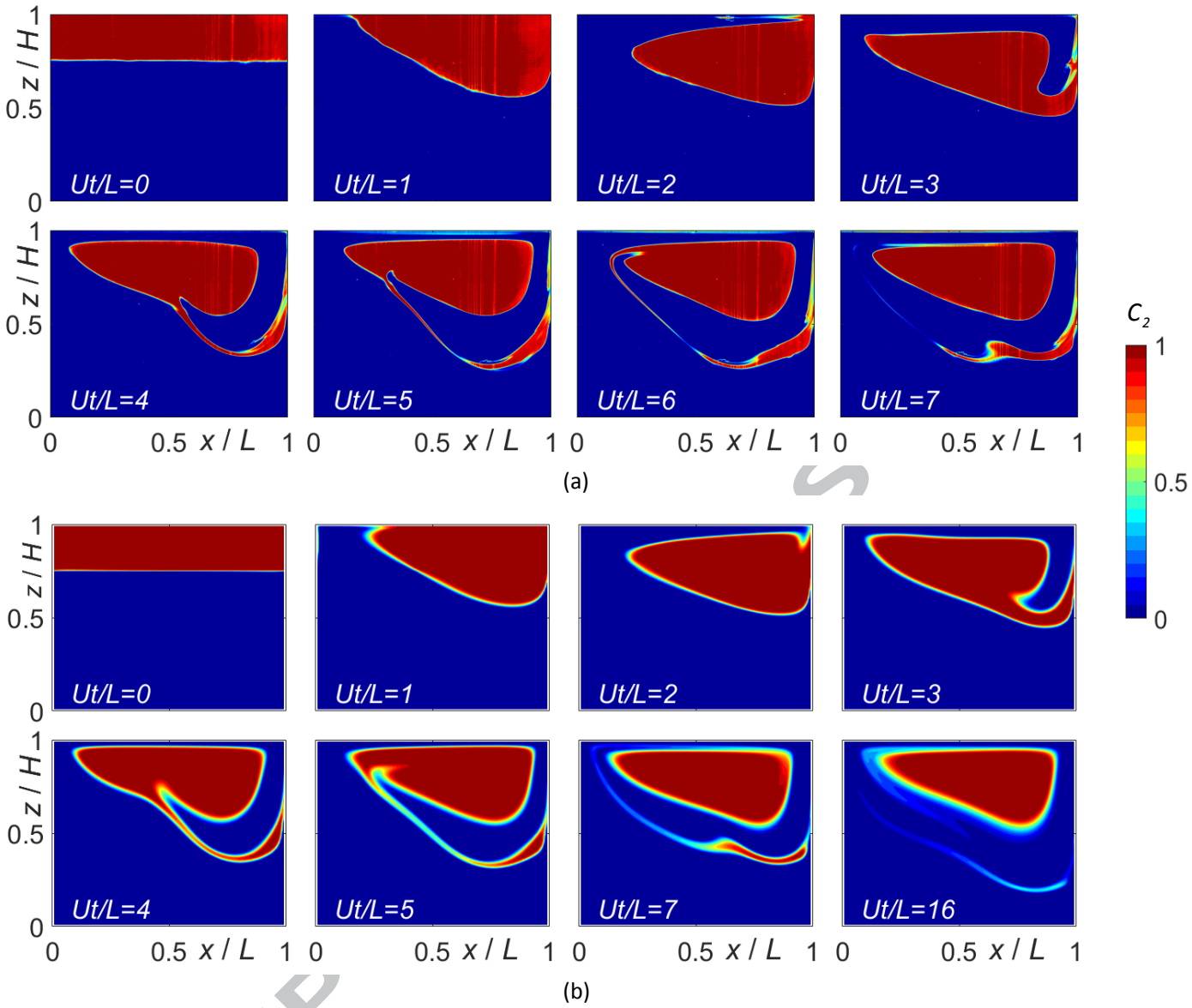

Fig. 5. (a) The instantaneous concentration of Liquid 2 measured in the experiments. (b) Simulated instantaneous concentration of Liquid 2 with 3.2 million cells.

Figure 6

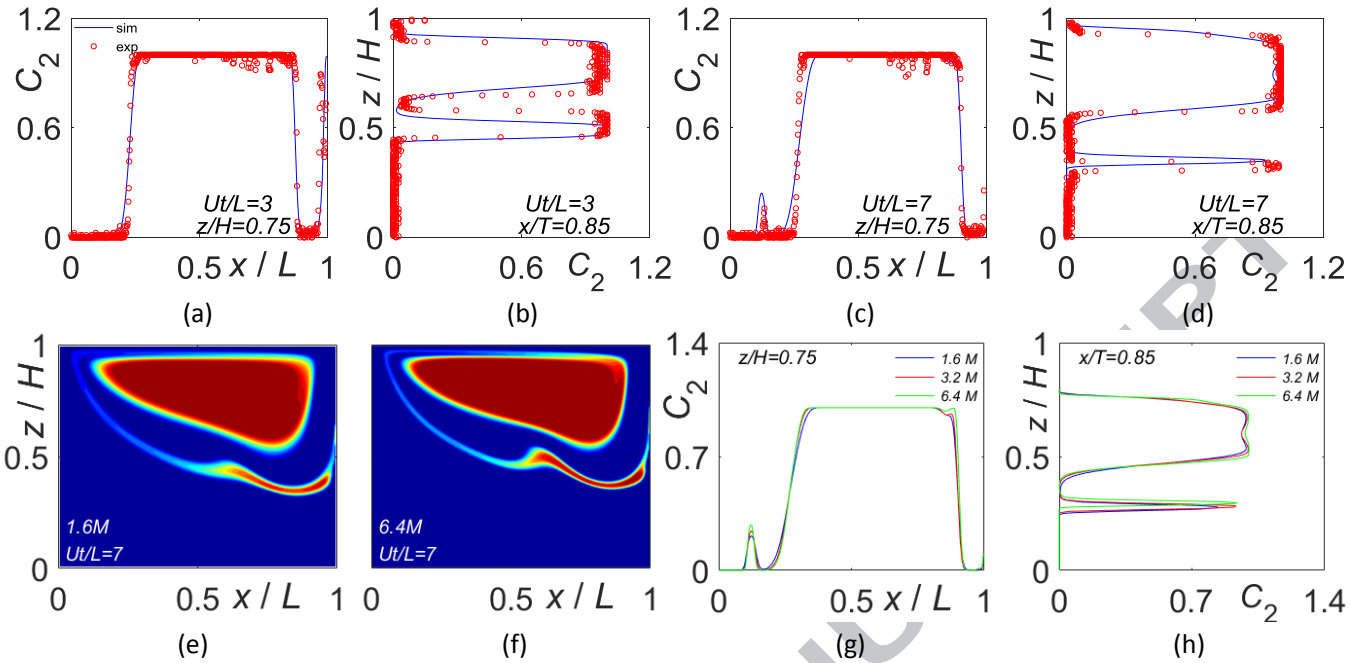

Fig. 6. Experimental and simulated concentration profiles of Liquid 2: (a) Ut/L= 3, z/H=0.75; (b) Ut/L= 3, x/T=0.85; (c) Ut/L= 7, z/H=0.75; (d) Ut/L= 7, x/T=0.85. Simulated concentration of Liquid 2 at Ut/L=7 with 1.6 million cells (e) and with 6.4 million cells (f). Effect of grid on the simulated concentration profiles of Liquid 2 at Ut/L=7 on lines z/H=0.75 (g) and x/T=0.85 (h).

Figure 7

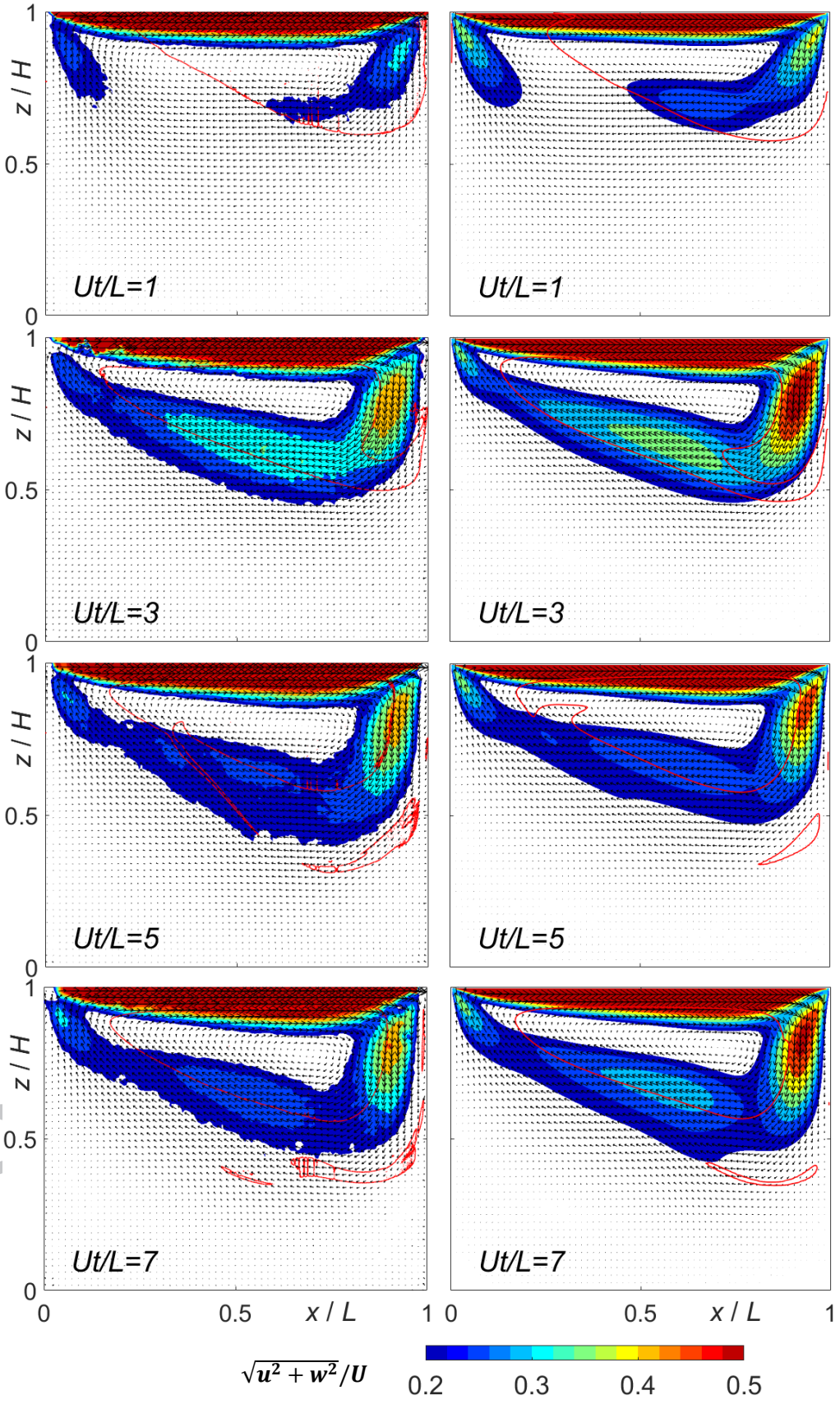

Fig. 7. Experimental (left column) and simulated (right column) instantaneous velocity field in the cavity with two miscible liquids. Only results at four moments are presented for conciseness. The distribution of Liquid 2 with volume fraction of 90 vol.% is marked by red lines in each panel. (ρ_1=1307 kg/m^3, ρ_2=1297 kg/m^3, μ_1=0.103 Pa·s, μ_2=0.079 Pa·s, U=0.02 m/s)

Figure 8

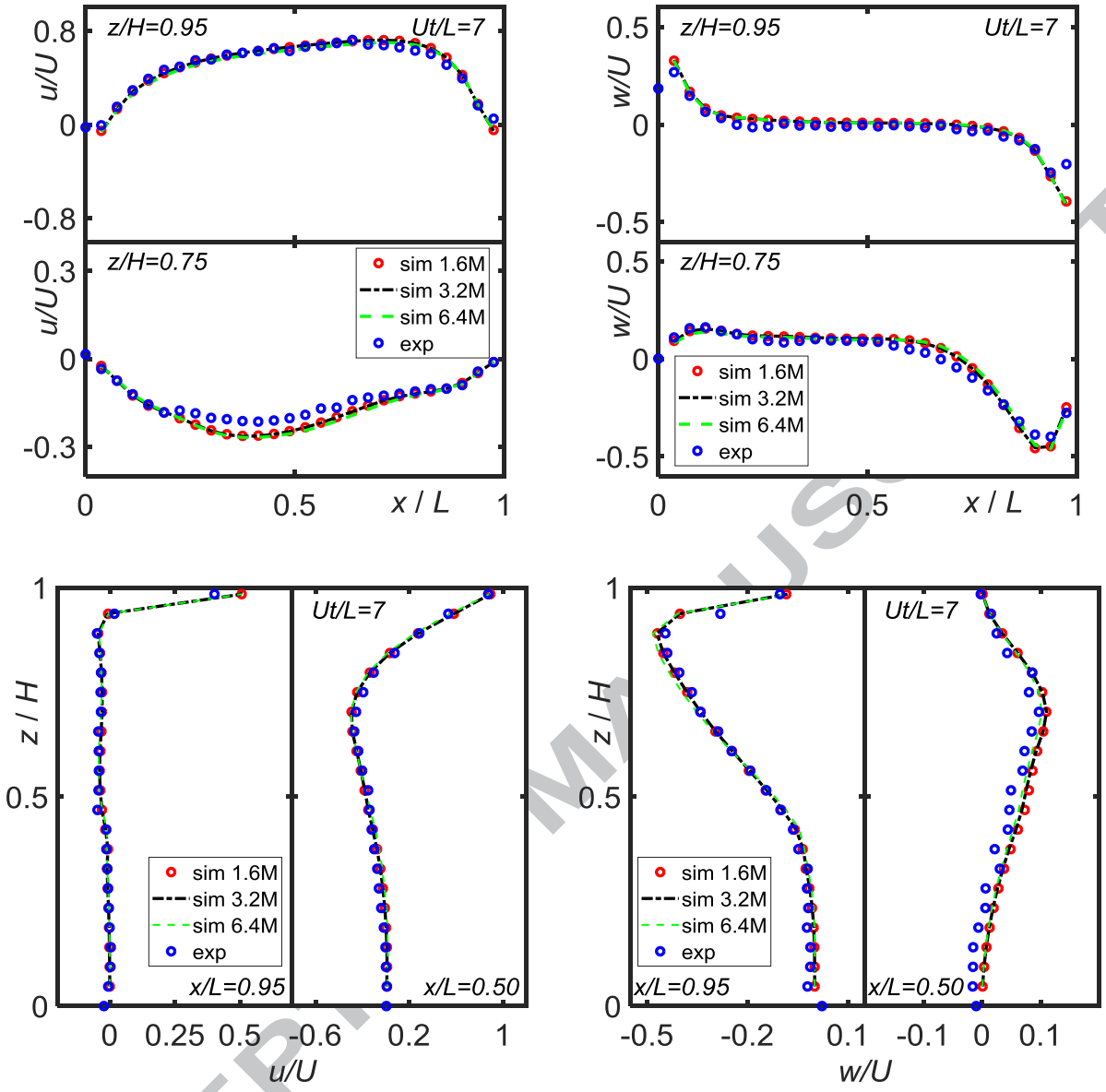

Fig. 8. Instantaneous velocity in *x* direction (left column) and in *z* direction (right column) at *Ut*/*L*=7 on two horizontal lines (*z*/*H*=0.75 and *z*/*H*=0.95) and two vertical lines (*x*/*L*=0.50 and *x*/*L*=0.95). The cavity was filled with two miscible fluids. Simulated results with 1.6, 3.2, and 6.4 million cells are shown in each panel.

Figure 9

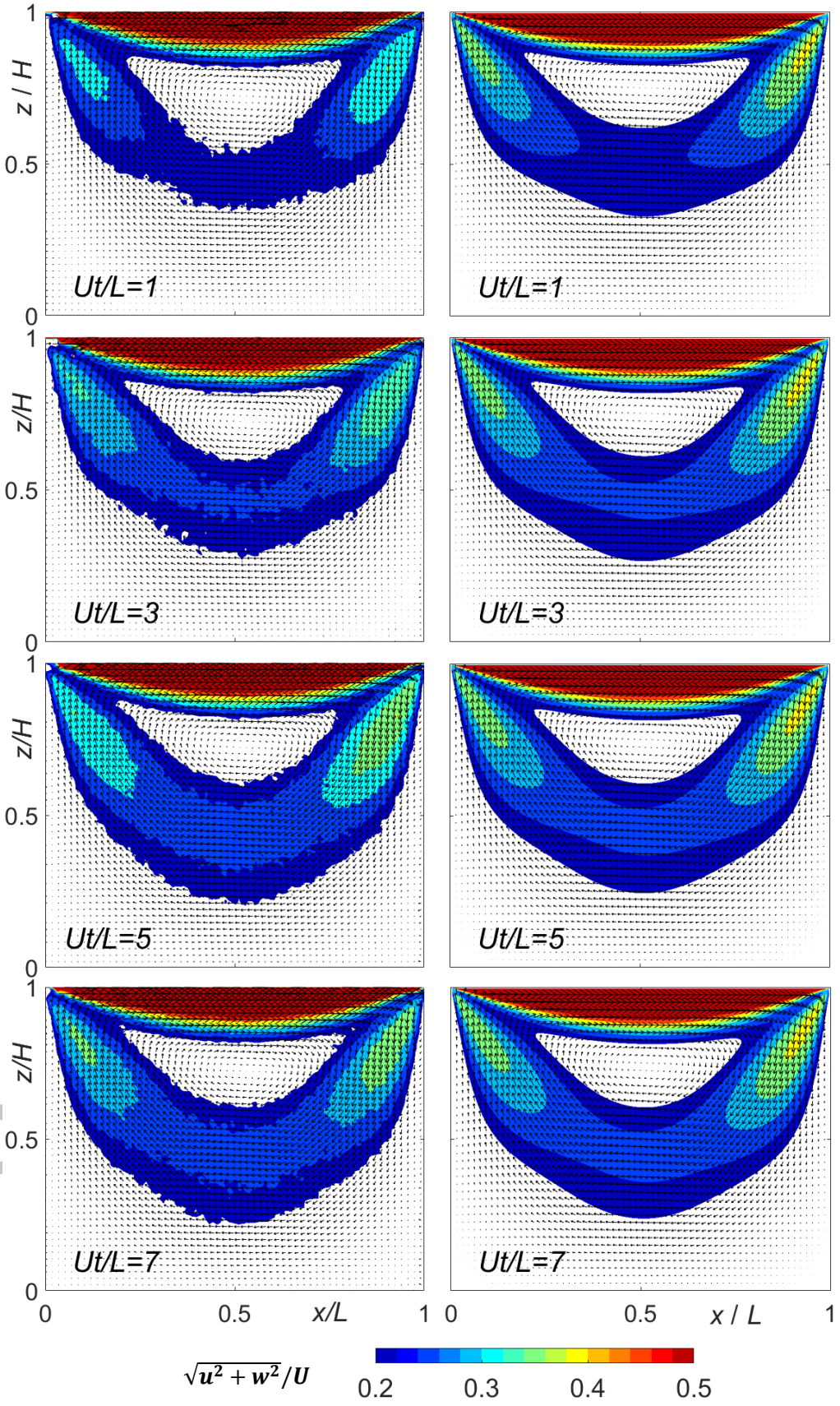

Fig. 9. Experimental (left column) and simulated (right column) instantaneous velocity field in the cavity with only Liquid 1. Only results at four moments are presented for conciseness. (ρ=1307 kg/m^3, μ=0.103 Pa·s, U=0.02 m/s)

Figure 10

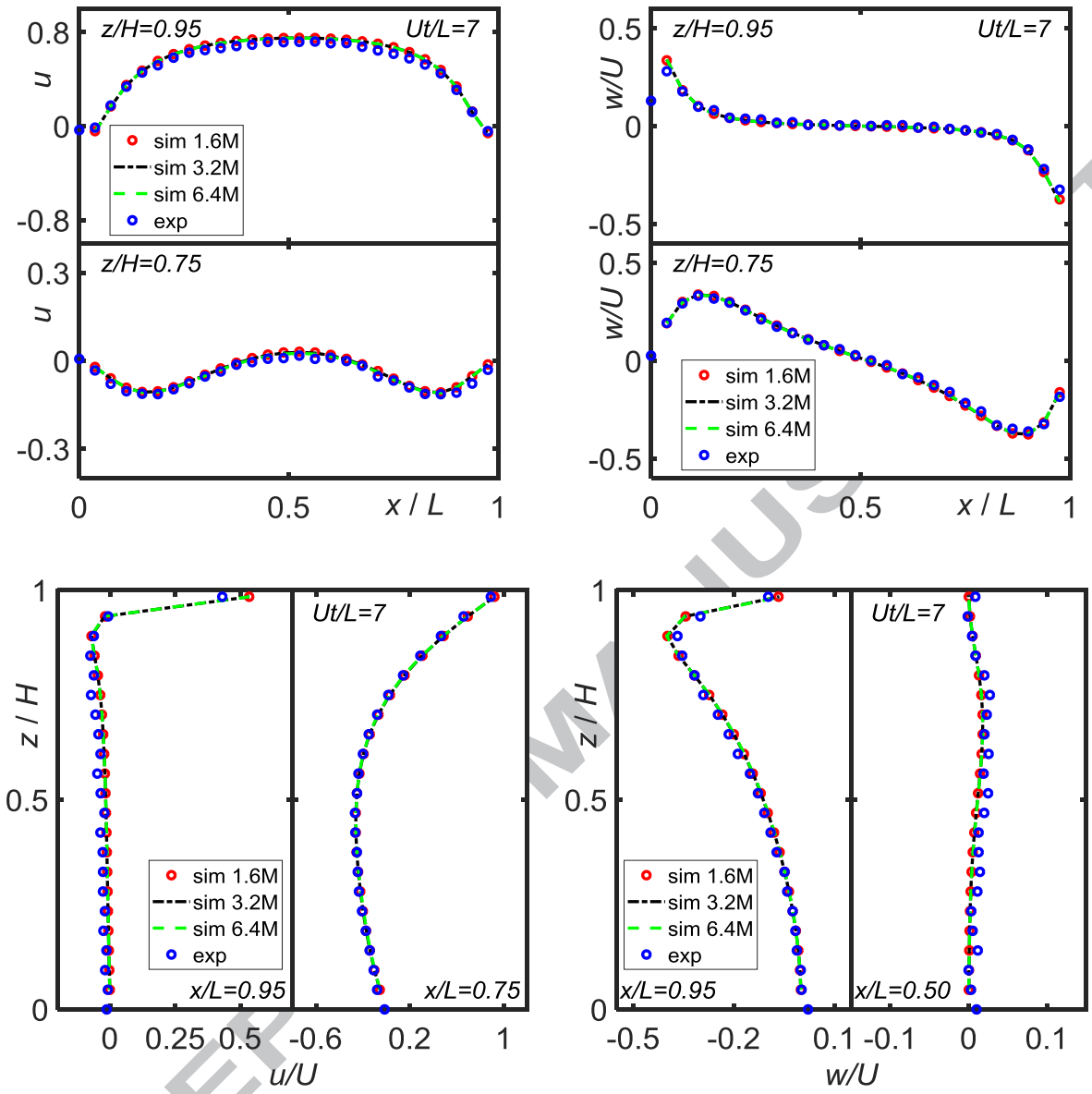

Fig. 10. Instantaneous velocity in *x* direction (left column) and in z direction (right column) at *Ut*/*L*=7 on two horizontal lines (*z*/*H*=0.75 and *z*/*H*=0.95) and two vertical lines (*x*/*L*=0.50 and *x*/*L*=0.95). The cavity was filled with only Liquid 1. Simulated results with 1.6, 3.2, and 6.4 million cells are shown in each panel.

Figure 11

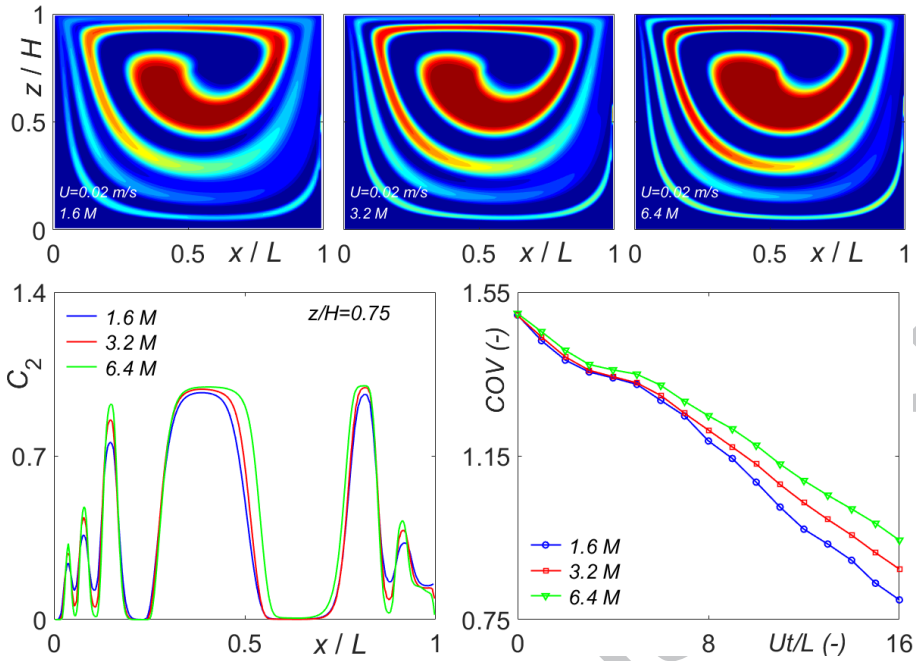

Fig. 11. Simulated concentration of Liquid 2 in the cavity at Ut/L=16 with 1.6, 3.2, and 6.4 million cells (top row). Quantitatively comparisons of the concentration profiles of Liquid 2 with $\frac{Ar}{Re}$=0 at Ut/L=16 on a horizontal line z/H=0.75 (bottom left). The instantaneous *COV* at $\frac{Ar}{Re}$=0 with 1.6, 3.2 and 6.4 million cells (bottom right).

Figure 12

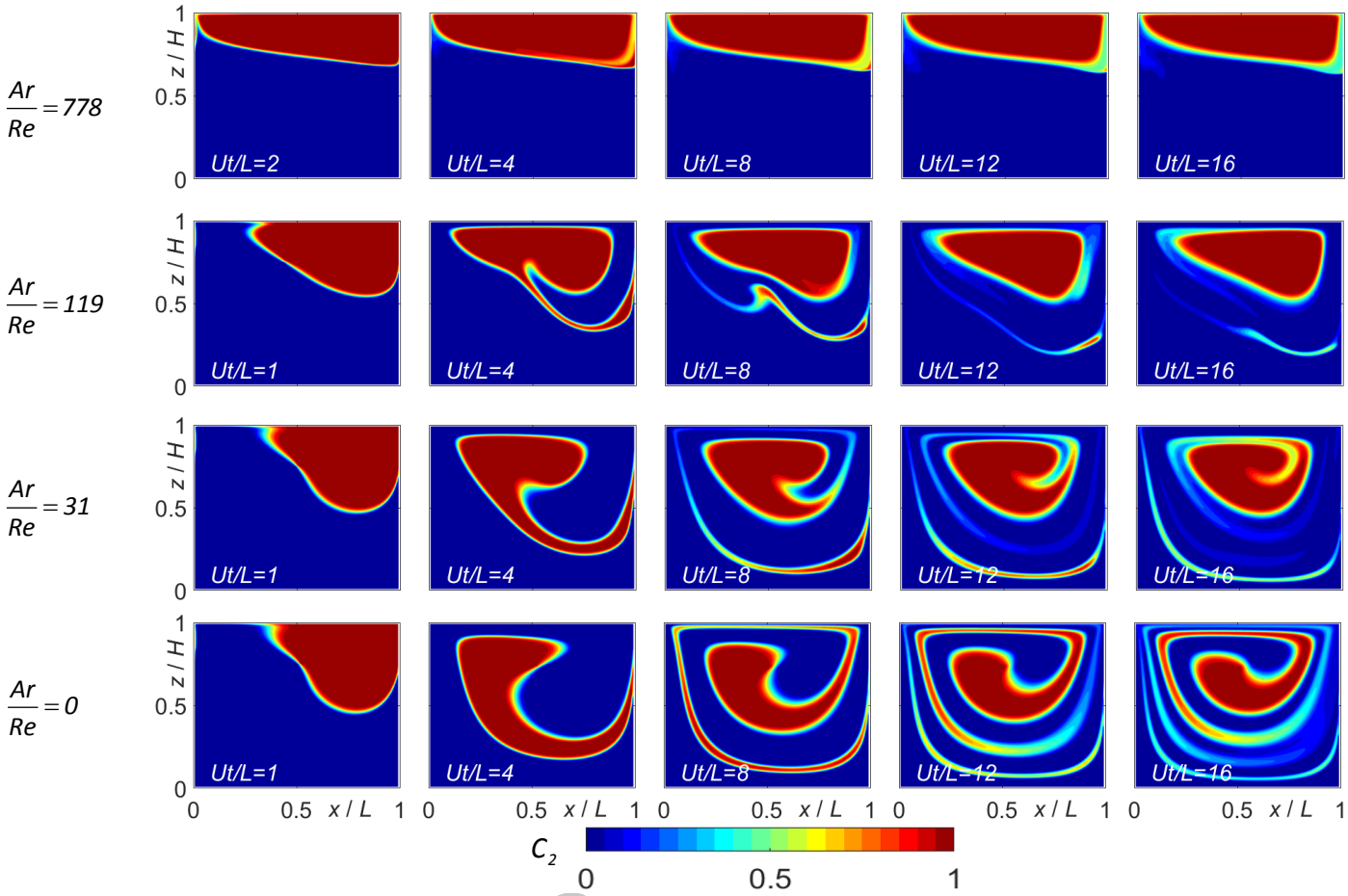

Fig. 12. Simulated instantaneous concentration of Liquid 2 in the cavity with two miscible fluids with different densities (and thus different $\frac{Ar}{Re}$). (ρ_1=1307 kg/m^3, ρ_2=1241.6, 1297, 1304.4, 1307 kg/m^3 (from top to the bottom), μ_1=μ_2=0.1030 Pa·s)

Figure 13

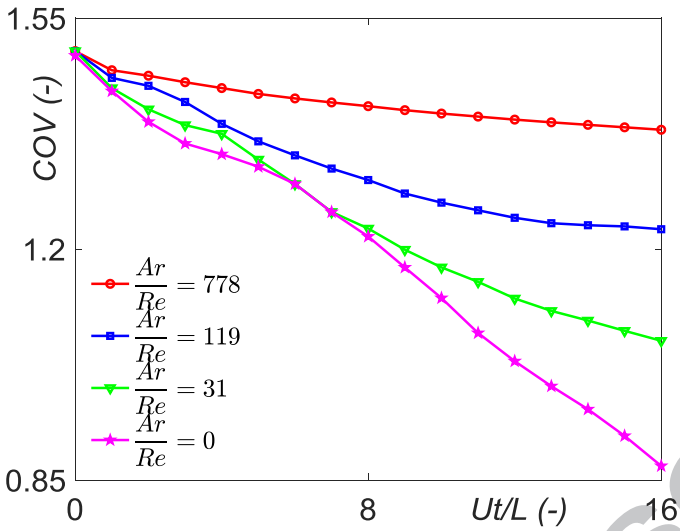

Fig. 13. Simulated instantaneous coefficient of variation in the cavity with two miscible fluids with different densities (and thus different $\frac{Ar}{Re}$). (ρ_1=1307 kg/m^3, ρ_2=1241.6, 1297, 1304.4, 1307 kg/m^3 (from top to the bottom), μ_1=μ_2=0.1030 Pa·s)

Figure 14

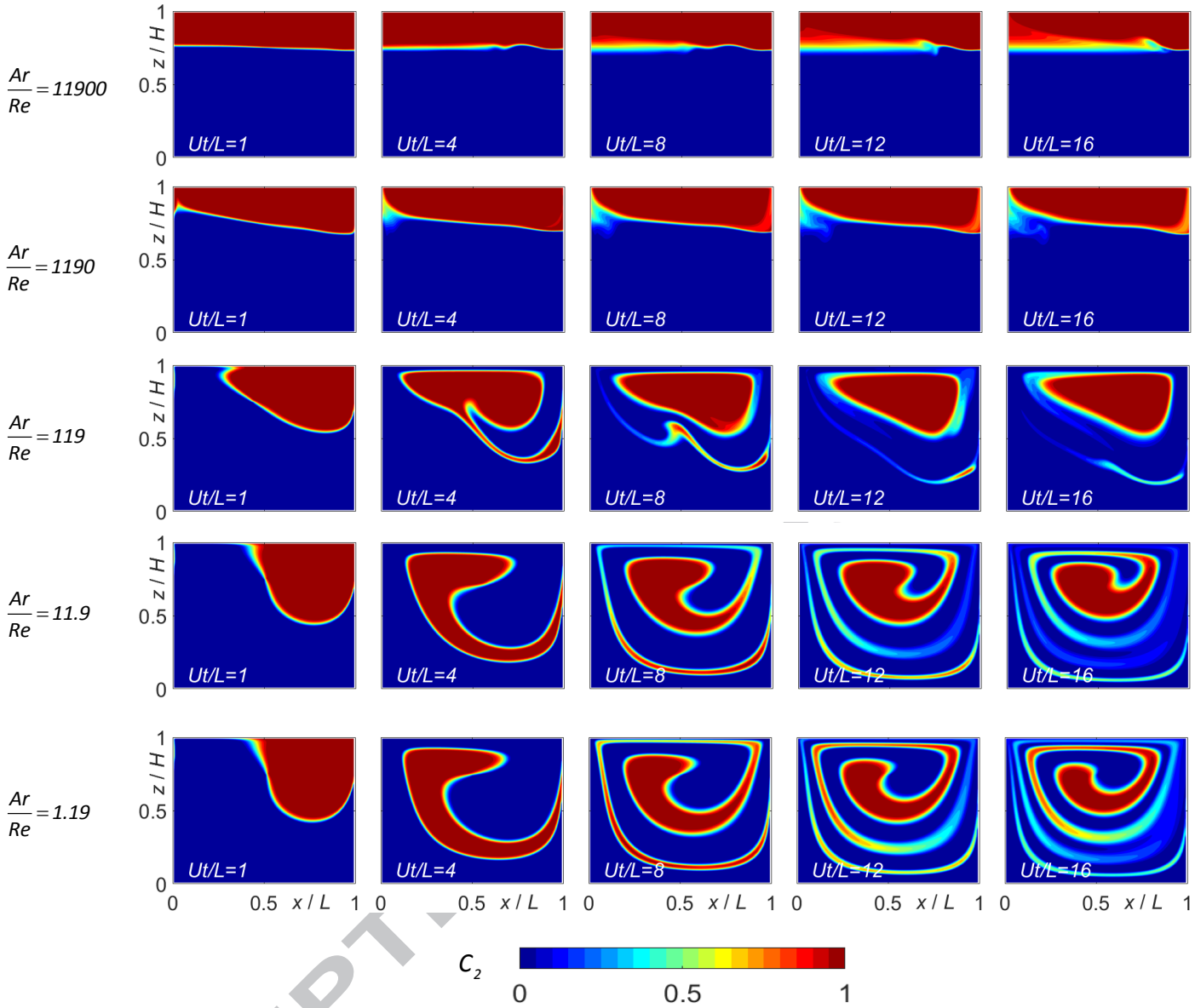

Fig. 14. Simulated instantaneous concentration of Liquid 2 in the cavity with two miscible fluids with different viscosities (and thus different $\frac{Ar}{Re}$). (ρ_1=1307 kg/m^3, ρ_2=1297 kg/m^3, μ_1=μ_2=0.00103, 0.0103, 0.103, 1.03,10.3 Pa·s (from top to bottom))

Figure 15

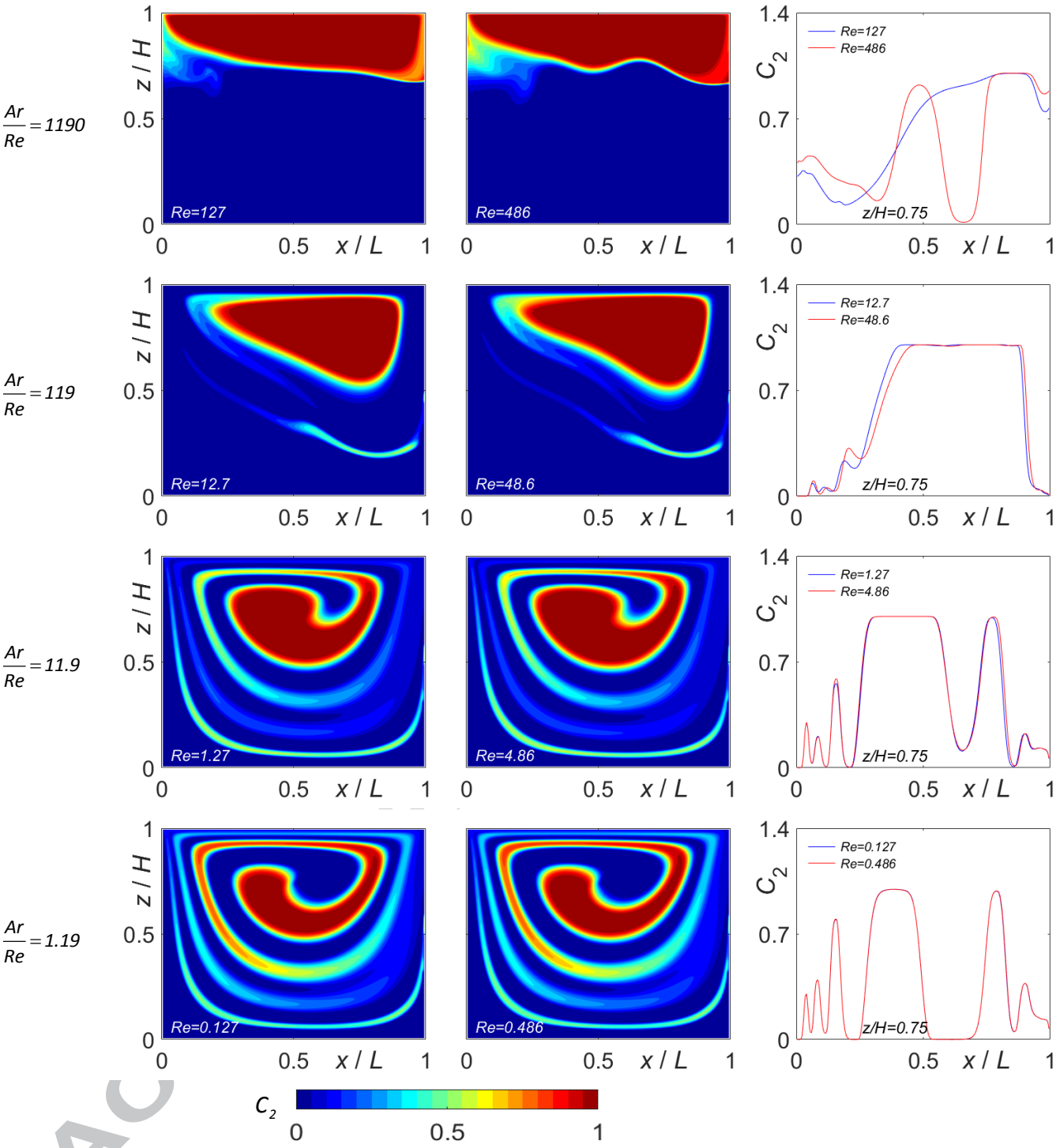

Fig. 15. Simulated concentration of Liquid 2 in the cavity at Ut/L=16. In each row, the values of $\frac{Ar}{Re}$ are the same. The right column quantitatively shows the concentration profiles of Liquid 2 with constant $\frac{Ar}{Re}$ on a horizontal line z/H=0.75.

Figure 16

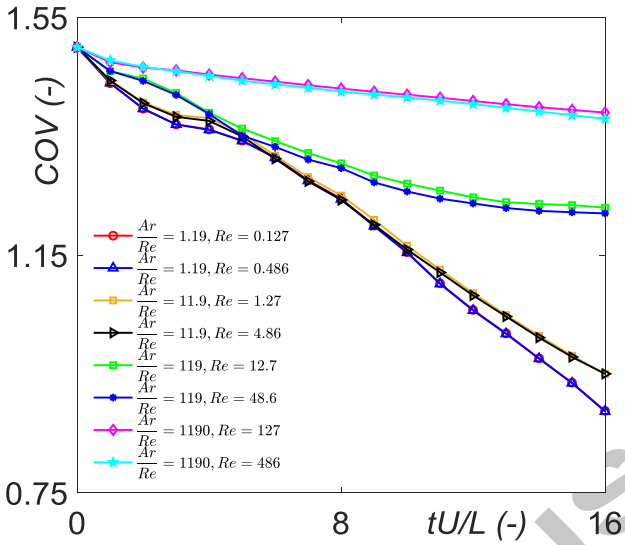

Fig.16. Simulated instantaneous coefficient of variation in the cavity with two miscible fluids with different $\frac{Ar}{Re}$.

Figure 17

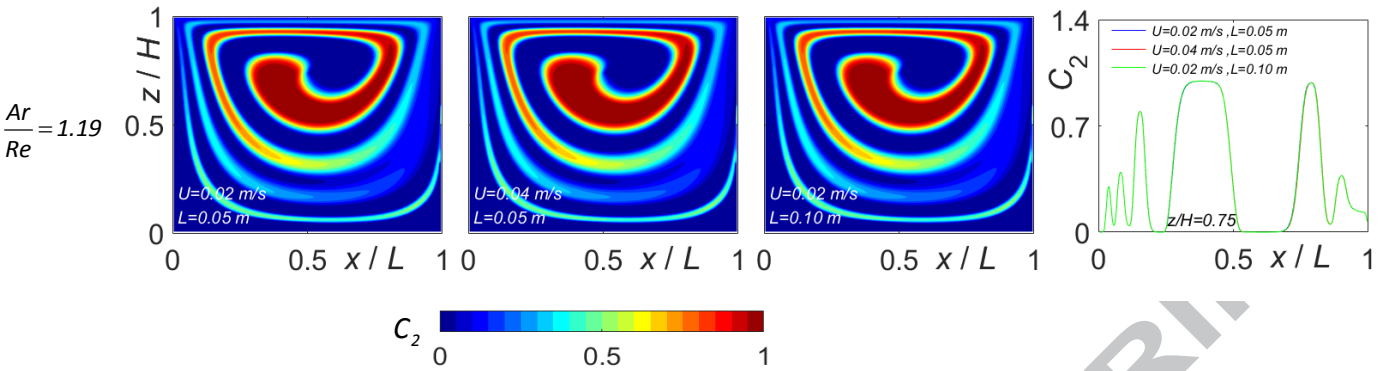

Fig. 17. Simulated Liquid 2 concentration in the cavity with $\frac{Ar}{Re}$=1.19 at Ut/L=16 with different U and L. The right column quantitatively shows the concentration profiles of Liquid 2 with the same $\frac{Ar}{Re}$ but different U and L on a horizontal line z/H=0.75. (ρ_1=1307 kg/m^3, ρ_2=1297 kg/m^3, μ_1=μ_2=10.3, 5.15, 41.2 Pa·s, Re=0.127, 0.508, 0.063(from left to right))